ACS APPLIED MATERIALS & INTERFACES

RESEARCH ARTICLE

www.acsami.org

Electrospun Carbon-Tin Oxide Composite Nanofibers for Use as Lithium Ion Battery Anodes

Christopher A. Bonino,[†] Liwen Ji,[‡] Zhan Lin,[‡] Ozan, Toprakci,[‡] Xiangwu Zhang,[‡] and Saad A. Khan[†,*]

[†]Department of Chemical and Biomolecular Engineering, North Carolina State University, Raleigh, North Carolina 27695-7905, United States

[‡]Department of Textiles Engineering, Chemistry, and Science, North Carolina State University, Raleigh, North Carolina 27695-8301, United States

Supporting Information

ABSTRACT: Composite carbon−tin oxide (C-SnO_2) nanofibers are prepared by two methods and evaluated as anodes in lithium-ion battery half cells. Such an approach complements the long cycle life of carbon with the high lithium storage capacity of tin oxide. In addition, the high surface-to-volume ratio of the nanofibers improves the accessibility for lithium intercalation as compared to graphite-based anodes, while eliminating the need for binders or conductive additives. The composite nanofibrous anodes have first discharge capacities of 788 mAh g^{-1} at 50 mA g^{-1} current density, which are greater than pure carbon nanofiber anodes, as well as the theoretical capacity of graphite (372 mAh g^{-1}), the traditional anode material. In the first protocol to fabricate the C-SnO_2 composites, tin sulfate is directly incorporated within polyacrylonitrile (PAN) nanofibers by electrospinning. During a thermal treatment the tin salt is converted to tin oxide and the polymer is carbonized, yielding carbon-SnO_2 nanofibers. In the second approach, we soak the nanofiber mats in tin sulfate solutions prior to the final thermal treatment, thereby loading the outer surfaces with SnO_2 nanoparticles and raising the tin content from 1.9 to 8.6 wt %. Energy-dispersive spectroscopy and X-ray diffraction analyses confirm the formation of conversion of tin sulfate to tin oxide. Furthermore, analysis with Raman spectroscopy reveals that the additional salt soak treatment from the second fabrication approach increases in the disorder of the carbon structure, as compared to the first approach. We also discuss the performance of our C-SnO_2 compared with its theoretical capacity and other nanofiber electrode composites previously reported in the literature.

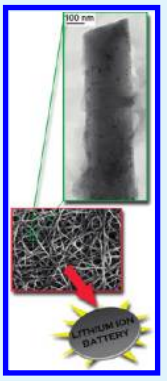

KEYWORDS: composite nanofibers, electrospinning, lithium-ion battery, tin oxide, anode

INTRODUCTION

Rechargeable lithium ion batteries (LIBs) have the potential to meet the power needs of future technologies, from portable electronics to plug-in electric vehicles (EVs). However, challenges remain that need to be overcome, in particular, development of lightweight and increased capacity materials for the anode, the negative electrode. One approach in this regard is to use elements that form alloys with lithium, such as tin (Sn) or silicon (Si), which have theoretical specific capacities 2−9 times greater than graphite (372 mA h g^{-1}), the current anode material.[1] However, anodes composed of lithium (Li) alloys may have poor cycle life as a result of large volume changes and pulverization during lithium de/insertion.[2] An alternative approach is to use blends of nanoscale alloys and carbon, which have complementary properties. Li-alloy nanomaterials are capable of better accommodating the strains from lithium de/alloying as compared to bulk materials and have high lithium capacities, whereas carbon has a good cycle life.[3,4] A carbon−lithium alloy-based anode material that is simple to fabricate and scale-up is therefore an attractive technology for future lithium batteries.

Electrospinning is an emerging process with applications for battery components, including separators and electrodes.[5−7] Electrospun fibers can be made with submicrometer diameters, with different functionalities and having high surface-to-volume ratios.[8−14] Battery electrodes with nanoscale features can have improved performance due to "short path lengths for electronic and Li ion transport." (reviewed in 15) In previous studies, tin-based[16] and carbon-based[5] nanostructured electrodes have performed better (i.e., higher rate capability) than conventional, macro-structured anodes. Furthermore, work by our group and others have shown that carbonized electrospun fibers with lithium alloys, including MnO_x, Fe_3O_4 and Si, can be used as LIB anodes.[17−23] Recently, tin salts have been electrospun with polymer fibers and converted to composite Sn-carbon anodes.[24−27] However, these approaches involved complicated fabrication steps, such as a coaxial electrospinning or heat treatment with a reducing atmosphere (i.e., hydrogen gas) that may be cumbersome for scalability. In addition, no attempt has been made to examine ways to enhance tin content in these systems.

We present two different approaches for fabricating electrospun carbon−tin oxide composite nanofibers, which are facile, tailor easily scalable and allows for incorporating additional tin-oxide on nanofiber surface. One method offers an in situ protocol to incorporate tin into the nanofibers, whereas the other scheme

Received: April 1, 2011
Accepted: May 26, 2011
Published: May 26, 2011

allows for enhancing tin content in the nanofibrous matrix via a simple post-treatment. In our first approach, solutions containing precursors to carbon fibers and tin oxide particles, PAN and tin sulfate, respectively, are electrospun. Following a series of thermal treatments in inert atmospheres, PAN is carbonized and the tin salt is converted to tin oxide by the following reaction

$$SnSO_4 + \text{heat} \rightarrow SnO_2 + SO_2 \quad (1)$$

[28]

The in situ incorporation of tin salts with the electrospinning process, and subsequent conversion by thermal treatment is a straightforward method to fabricate functional composite nanofibers. The composite carbon−tin oxide (C-SnO_2) fiber mats are then used directly as lithium-ion battery anodes. The mechanical stability and good conductivity of the carbon nanofibers allow the elimination of polymer binders and conductive fillers, reducing nonactive material in the electrode. The addition of SnO_2 raises the storage capacity of the nanofibrous anode. Lithium can react with tin oxide to form an alloy by the following scheme[29]

$$\begin{aligned} SnO_2 + 4Li^+ + 4e^- &\rightarrow 2Li_2O + Sn \\ Sn + xLi^+ + 4e^- &\leftrightarrow Li_xSn (0 < x \leq 4.4) \end{aligned} \quad (2)$$

For the second approach, we modified our fabrication strategy to enhance the loading of tin oxide particles. The electrospun PAN/$SnSO_4$ nanofibers were thermally treated in air to stabilize the polymer, after which, the nanofibers mats were infiltrated with tin sulfate by an aqueous soaking treatment. The samples were then thermally treated to carbonize the polymer and convert the salt to SnO_2. The salt-soak treatment in this study results in composite nanofibers with their outer surfaces loaded with SnO_2 nanoparticles. Having lithium alloys accessible at the fiber surface is advantageous for Li-ion anodes, since the lithium can be stored at the electrode surfaces. After fabrication, we evaluated the anode performance of the solution-soaked carbon mats. In a previous study by Lee, et al., SnO_2-coated, colloidal sphere-templated structures were prepared from a tin sulfate solution soak and decomposition heat treatment.[30] However, when evaluated as LIB anodes, the specific capacities were fairly low (<300 mA h g^{-1} at 25 mA g^{-1} current density). Our composite C-SnO_2 nanofibers require fewer process steps, and have higher capacities. To the best of our knowledge, we are the first to use a salt-soaking treatment to fabricate composite electrospun mats used as LIB anodes.

EXPERIMENTAL SECTION

Materials. Polyacrylonitrile (PAN, M_W = 150 000 g/mol, Scientific Polymer Products), *N*,*N* dimethylformamide (DMF, Fisher Scientific), and tin sulfate (Gelest) were used as received.

Methods. *Preparation of PAN/Tin Salt Solutions.* Polymer solutions were prepared by adding tin sulfate (2 wt %) and PAN (7.5 wt %) into DMF and stirring with a magnetic stir bar overnight at 60 °C. The solution was sonicated for 10−15 min prior to electrospinning to disperse the salt particles.

Solution Characterization. Steady shear rheology experiments were performed at 25 °C using a stress-controlled rheometer (AR2000, TA Instruments) with a 40 cm, 2° cone and plate geometry, and applying stresses ranging from 0.01−100 Pa (10 points per decade). Zero shear viscosities were estimated by averaging the first 10 points of the Newtonian regime. Ionic conductivity was determined using a potentiostat (Gamry Instruments) and correlating with a standard (1 mS/cm) potassium chloride (Fisher Scientific). Surface tension was measured from a pendant drop analyzer from SEO Co. Ltd. (model Phoenix 300).

Preparation of Carbon−Tin Oxide Nanofibers. Polymer nanofibers were prepared by electrospinning. PAN solutions were pumped through a 10 mL syringe fitted with a 22 gauge needle at a flow rate of 0.5 mL/h. The distance between the collector plate and needle was fixed at 15 cm with a 7−8 kV applied voltage. Details of the setup are described elsewhere.[8−12] Approximately 50 μm thick mats were prepared by electrospinning for ∼18 h in an ambient environment with 40−55% relative humidity. As-spun fiber mats were heated in a furnace in air at 2 °C/min up to 280 °C, and held constant for 6 h to stabilize the PAN. Subsequently, the furnace was purged with nitrogen and heated at a rate of 2 °C/min. The final temperature of 600 °C was maintained for 8 h for the carbonization.

Characterization of Polymer and Carbon Composite Fibers. Polymer and heat-treated fibers were characterized using a field emission scanning electron microscope (FE SEM, FEI XL30, 5 kV accelerating voltage, beam spot size 3, 5−7 mm working distance, Ultra High Resolution mode). Prior to analysis, polymer fiber mats were sputter-coated with 7−10 nm of gold. The diameters and standard deviations of 50 fibers per sample, without bead defects, were measured using Adobe Photoshop CS3. Carbon fiber mats that were not evaluated for diameter measurements were not sputter coated. Quantitative elemental analysis was characterized using a SEM (Hitachi S-3200N, 10 kV accelerating voltage, current setting 50, 18−20 mm working distance) with energy-dispersive spectroscopy (EDS) system.

Fibers were also electrospun directly onto grids and analyzed with a transmission electron microscope (TEM, Hitachi HF2000 with EDS, 200 kV accelerating voltage). Fiber crystalline structure was measured using an X-ray Diffractometer (Philips X'Pert PRO MRD HR) and a Raman spectrometer (Horiba, 633 nm laser). Lorentzian distribution curves were fit to Raman spectra using Origin 8. Peak intensities and ratios were averages from three spectra for each sample.

Evaluation of Fiber Mats as Li-Ion Battery Anodes. Carbonized mats were punched out to the appropriate dimensions for 2032 coin-type cells. Battery cells contained fiber mats attached to copper foil (Lyon industries) as the working electrode and lithium ribbon (Aldrich) as the counter electrode. The separator and electrolyte were Separion S240 P25 (Degussa) and 1 M lithium hexafluorophosphate ($LiPF_6$) in 1:1 (v/v) ethylene carbonate/ethyl methyl carbonate (Ferro Corporation), respectively. After assembly, the half cells were cycled between 2.80 and 0.02 V using an automatic battery cycler (Arbin). Cycling current densities included 50, 100, 200, 300, or 500 mA g^{-1}.

RESULTS AND DISCUSSIONS

1.1. Carbon-SnO_2 Nanofibers by In situ Electrospinning. In our first approach, solutions containing PAN and $SnSO_4$ were electrospun into nanofibers. C-SnO_2 composites were then prepared by heating the polymer−salt nanofibers in a controlled-atmosphere furnace. As a first step, we examined properties of nanofibers prior to carbonization. Salt-free PAN nanofibers were used as a control. Figure 1b-d reveal that nanofibers obtained from both solutions (with and without salt) have similar-sized diameters, 293 ± 67 nm and 298 ± 57 nm, respectively. However, the addition of $SnSO_4$ to the PAN solution causes more bead defects. Analysis with TEM reveals what may be salt particles on and beneath the surface of the PAN fibers containing $SnSO_4$; no particles are observed on the pure PAN fibers (Figure 1e, f).

The properties of electrospinning solutions can be related to the morphology of electrospun fibers. In particular, solution viscosity, ionic conductivity, and surface tension affect the ability of a solution to be electrospun.[31] Table 1 shows that PAN

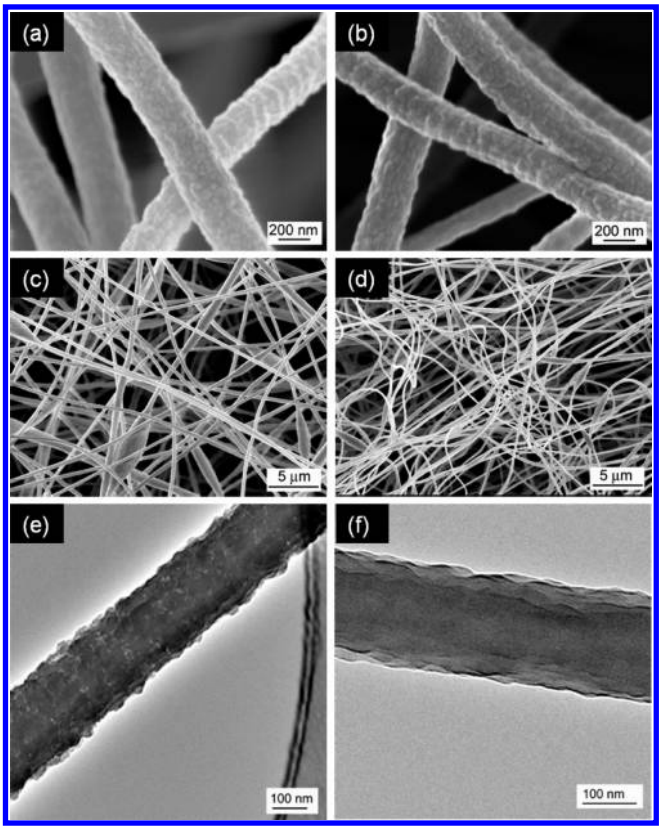

Figure 1. Electron micrographs of electrospun PAN nanofibers with (a, c, e) and without (b, d, f) tin sulfate. Figures a−d were captured with SEM and e and f with TEM. Average fiber diameters were 293 ± 67 and 298 ± 57 nm, respectively. The SEM samples were sputtered-coated with gold.

Table 1. Properties of Electrospun Solutions

	PAN solution	PAN + $SnSO_4$ solution
zero shear viscosity (Pa s)	0.47	0.50
conductivity (mS/cm)[a]	0.03 ± 0.01	0.11 ± 0.01
surface tension (mN/m)[a]	33 ± 3	33 ± 2

[a] Means ± standard deviations are reported using a sample size of 5 measurements.

solutions containing $SnSO_4$ have a greater ionic conductivity than pure PAN solutions, which can be attributed to the dissociation of the salt. Both solutions have surface tensions ~33 mN/m, which indicates that PAN has a greater affinity for the air−DMF interface than $SnSO_4$. In addition, zero shear viscosities are comparable, indicating that salt has minimal effects on the stability of PAN in DMF, unlike what has been seen with other salts (e.g., $AlCl_3$).[32]

C-SnO_2 composites were prepared by heating the polymer-salt nanofibers in a controlled-atmosphere furnace. Fibers mats were stabilized at 280 °C in air, which cross-linked the PAN chains through dehydrogenation and cyclization reactions.[33] The next thermal treatment was performed in a nitrogen atmosphere at 600 °C, during which, two conversion reactions occurred. First, the polymer precursor was carbonized, resulting in the release of the gases, which include methane, hydrogen, hydrogen cyanide, water, carbon dioxide, and/or ammonia.[34] During this

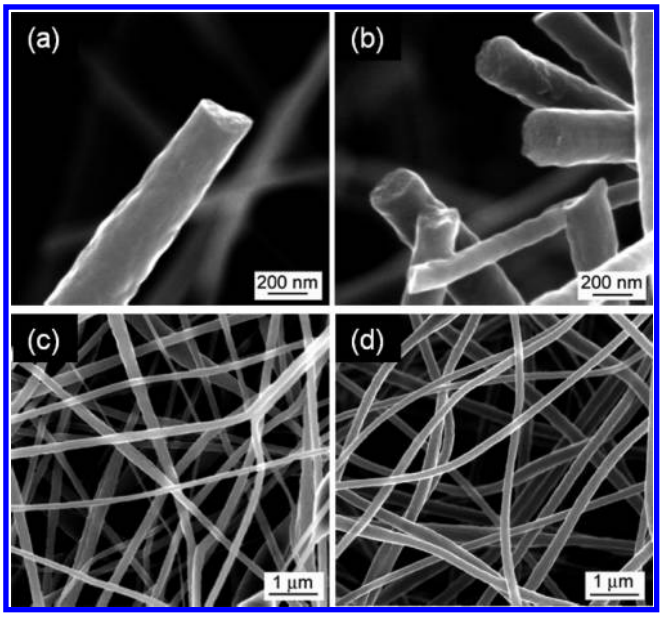

Figure 2. Scanning electron micrographs of carbonized nanofibers (a, c) with and (b, d) without tin oxide. Average fibers diameters were 176 ± 36 and 223 ± 38 nm, respectively. The samples were not sputtered-coated.

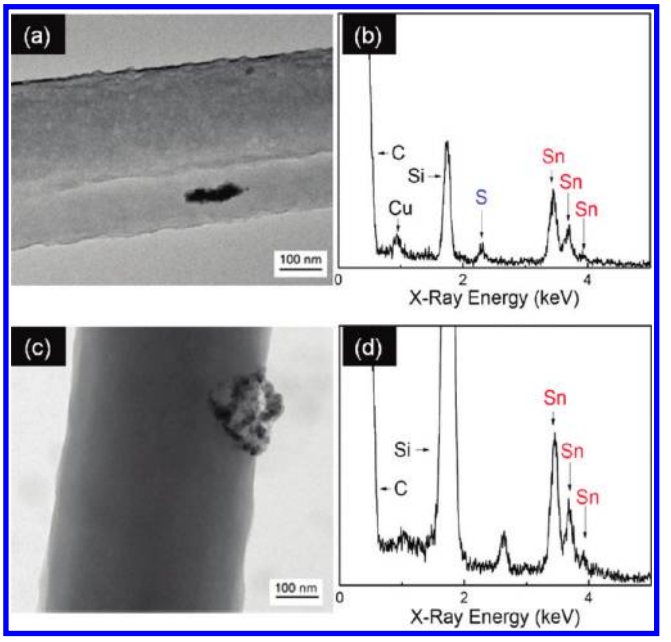

Figure 3. Transmission electron micrographs of composite fibers after (a) stabilization and (c) carbonization heat treatments, and corresponding energy dispersive spectra (b and d, respectively). The presence of Sn and S in spectrum b indicates that tin sulfate has not been converted to tin oxide during the stabilization. In comparison, the absence of S in spectrum d indicates that SnO_2 has formed. The peak near 2.7 eV is an artifact of the strong Si peak from the TEM grid.

treatment, the mat color changes to black. The second outcome of the heat treatment is that the tin sulfate salt was converted to tin oxide, following the reaction in eq 1.

1.2. Characterization of Stabilized and Carbonized Nanofibers. The C-SnO_2 and carbon fibers were characterized to

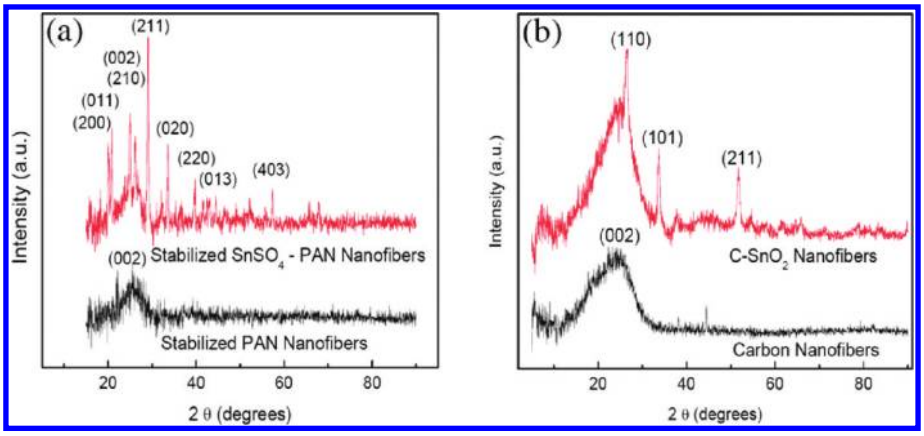

Figure 4. X-ray diffraction patterns of fibers after (a) stabilization heat treatment and (b) carbonization heat treatments. Fibers containing the tin salt show a change in crystal structure from $SnSO_4$ (JCPDS no. 16−0252) to SnO_2 (JCPDS no. 41−1445).

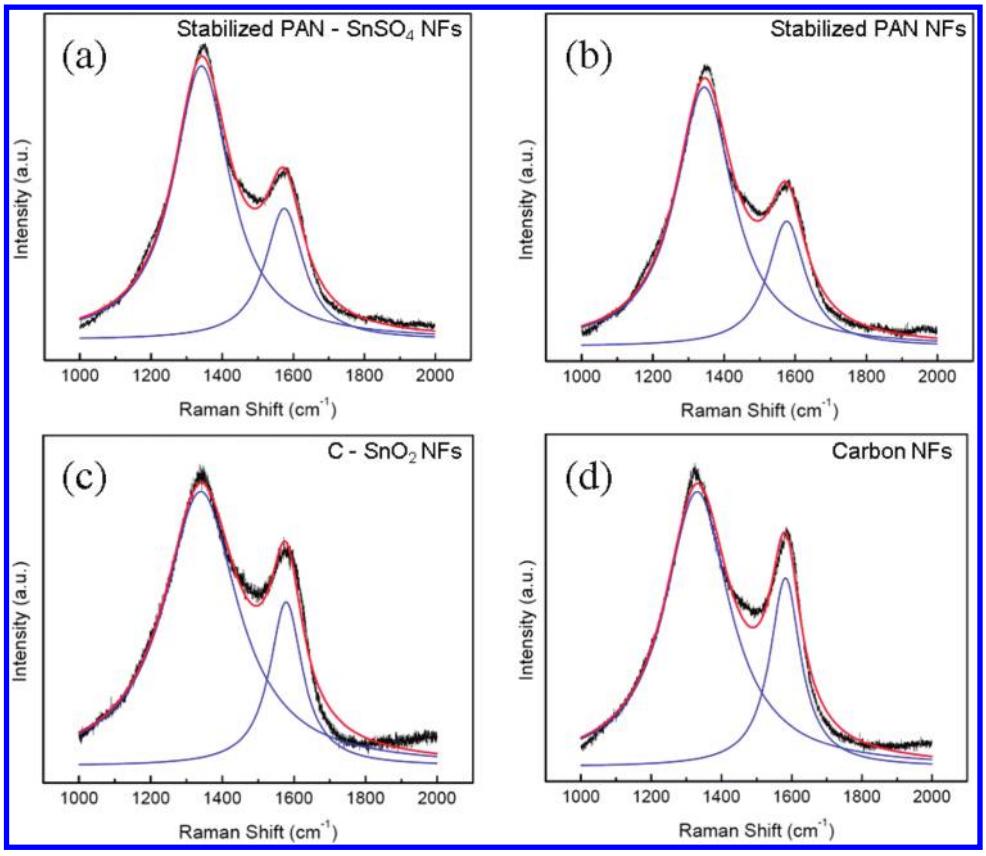

Figure 5. Raman spectra of (a) stabilized PAN/$SnSO_4$ (b), stabilized PAN, (c) carbonized PAN/$SnSO_4$, and (d) carbonized PAN fiber mats. The disordered (D) and graphitic (G) peaks centered at ∼1340 and ∼1580 cm^{-1} were fit to the spectra using Lorentzian distributions. Height ratios, $I(D)/I(G)$ are 2.1 ± 0.1, 2.1 ± 0.1, 1.6 ± 0.1, and 1.5 ± 0.2, respectively.

identify structural changes from their conversion. SEM analysis reveals that the C-SnO_2 and carbon fibers have smaller diameters (176 ± 36 and 223 ± 38 nm, respectively) than the polymer fibers due to the release of gases (e.g., NH_3) and resulting fiber mass reduction during the carbonization process.[5,35] In order to examine the presence of SnO_2, the carbonized fibers were observed without a conductive coating by SEM because the absence of gold-coating allows for a better contrast and ease in identifying more electron dense materials (i.e., SnO_2 particles) on the carbon fiber surfaces. (Figure 2.) The outer surfaces and cross sections of carbon fibers with and without the tin salt have similar appearances; SnO_2 particles are not apparent in the scanning electron micrographs. However, TEM analysis reveals that aggregates of particles with 15−20 nm diameters are present within the fibers after the stabilization and carbonization heat treatments. (Figure 3.) Using energy-dispersive spectroscopy (EDS) we found that the particle aggregates contained tin with and without sulfur, before and after the carbonization heat treatment, respectively. The absence of sulfur after the final thermal treatment indicates that tin sulfate was converted to tin

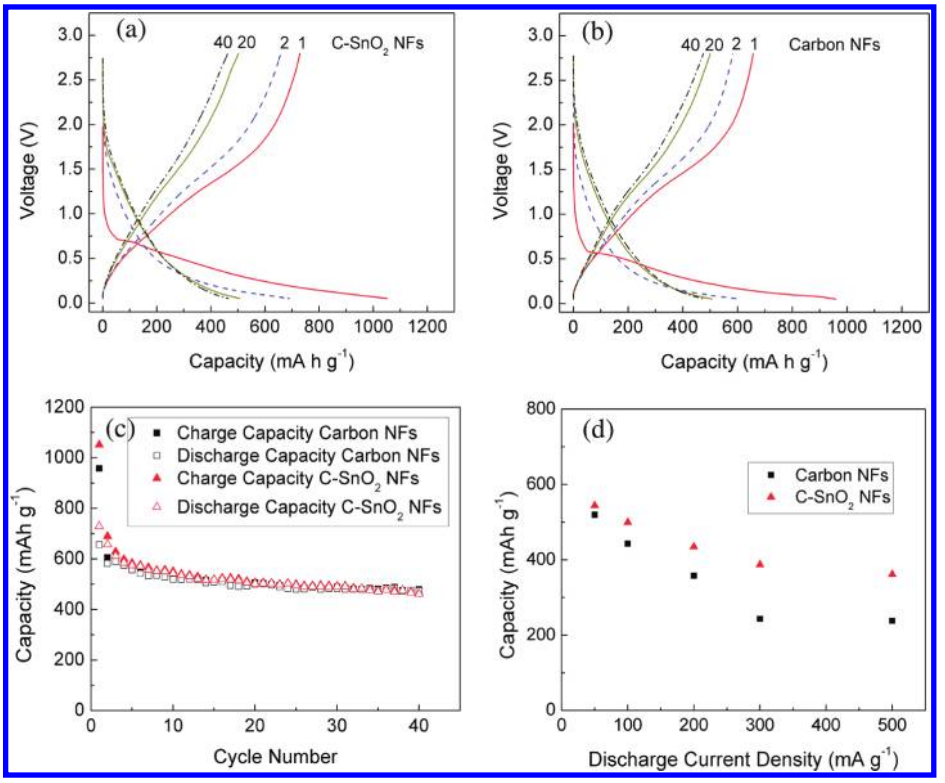

Figure 6. Performance of composite and carbon nanofiber mats as anodes in lithium ion battery half cells. Charge−discharge curves for (a) C-SnO_2 and (b) carbon nanofiber anodes cycled between 0.05 and 2.80 V (vs Li/Li^+) at the rate of 50 mA/g. Curves at 1st, 2nd, 20th, and 40th cycles are shown. (c) Cycle performance at 50 mA g^{-1} current density and (d) rate capability at 10th cycle for C-SnO_2 composite anodes in Li-ion battery half cells.

oxide. The peak near 2.7 eV is an artifact of the strong Si peak from a silicon nitride TEM grid.

XRD analysis confirmed the TEM/EDS results on the formation of tin oxide during the final heat treatment. Figure 4a and b show X-ray diffractograms of the fiber mats after the stabilization and carbonization treatments, respectively. Stabilized PAN/$SnSO_4$ nanofibers have characteristic peaks that can be assigned to tin sulfate (JCPDS no. 16−0252), whereas no tin oxide peaks are found. This result confirms that tin sulfate is not converted to tin oxide during the stabilization heating condition (280 °C in air). After the carbonization, the composite fiber patterns contained prominent peaks at near 26, 33, and 52°, which were indexed to the (110), (101), and (211) planes of SnO_2 (JCPDS no. 41−1445). Additionally, a broad peak was present at 2θ = 25° on both the C-SnO_2 and carbon samples, corresponding to the (002) diffraction peak of graphite, which indicates the formation of carbon.

The microstructure of the carbon fibers changed throughout the heat treatments, as revealed by Raman spectroscopy. Shown in panels a and b in Figure 5 are representative Raman spectra of stabilized composite and pure fibers that exhibit two broad peaks. The peaks centered at ∼1340 and ∼1580 cm^{-1} correspond to D and G bands of disordered carbon, respectively.[36] The presence of these two peaks indicates that the PAN polymer chains reacted to form ring structures with sp^2 and sp^3 bonding. Because the fibers were not yet heated under nitrogen at elevated temperatures for carbonization, the stabilized fibers contain nitrogen, hydrogen, and oxygen, in addition to carbon, as reviewed by Rahaman et al.[34] The presence of noncarbon bonds may disrupt ordering of the aromatic rings, leading to disordered carbon structures with small ring clusters. To characterize the fiber microstructure, two Lorentzian curves were fit to the spectra. The ratio of the peak intensities I_D/I_G, known as R, characterizes the extent of structural disorder within carbon and is inversely proportional to cluster size of the aromatic rings in noncrystalline graphite materials ($R \approx 1/L_c$).[36] Peak ratios of the stabilized fibers were 2.1, verifying the highly disordered structure. R values were the same for stabilized fibers with and without salt. Thus, the $SnSO_4$ incorporated within the fibers during electrospinning did not affect the hydrocarbon fiber microstructure.

The carbonization heat treatment increased the ordering and cluster sizes of the fiber mats. By our estimates, both samples of carbonized nanofibers had comparable R values, 1.5 − 1.6, which indicate a disordered graphitic structure with small cluster domains. Previous work by Zussman, et al. has reported R < 1.0 in carbonized PAN nanofibers.[37] However, differences in methodologies between our studies may explain the discrepancies. For example, the carbonization temperature in our study was 100 °C lower, which likely contributed to the more disordered structure.[38]

1.3. Performance of C-SnO_2 Nanofiber Mats as Li-Ion Battery Anodes. The nanofiber mats were evaluated as anodes in Li-ion battery half cells. The conductive nanofiber mat provided ample mechanical structure, eliminating the need for conductive additives (e.g., carbon black) or binders. Mats containing tin oxide achieved higher performances as compared to the pure carbon nanofibers. Shown in Figure 6a and b are representative charge−discharge curves for pure carbon and tin oxide-carbon nanofiber anodes. The initial rapid reduction in voltages from 2.8 to ∼0.6 V during the first charge cycles (C1) are due to the formation of a solid electrolyte interface (SEI) film on the anode.[39] The SEI film is caused by an irreversible reaction

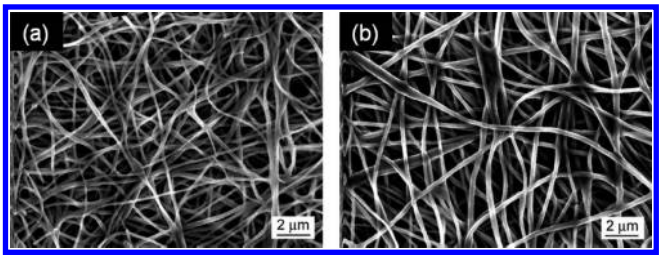

Figure 7. Micrographs of (a) C-SnO_2 and (b) carbon fiber anodes after 40 cycles, verifying the mats maintain their structure during lithium de/insertion. The samples were not sputtered-coated.

of lithium with the electrolyte to yield compounds that include Li_2O and LiF.[40,41] C1 curves of the carbon and tin oxide-carbon have plateaus 0.55 and 0.70 V, respectively, which are attributed to the formation of carbon- and/or tin−lithium alloys.[1] The C-SnO_2 anode has a greater first discharge capacity than the carbon fiber anode, 700 versus 620 mA h g^{-1}, respectively, because tin alloys can accommodate more lithium than carbon sheets. Both anodes materials have comparable Columbic efficiencies (70%) in their first cycles, which were attributed to the formation of the SEI film on the fiber surfaces.[39] After subsequent cycles at a constant current density of 50 mA g^{-1}, the capacity of the composite anode approaches the capacity of the pure carbon, which may be the result of damage to tin oxide from volume changes during lithium insertion.[42] (Figure 6c) However, the 40th cycle capacity of both anode materials are ~470 mA h g^{-1}, which exceed the theoretical capacity of graphite by 100 mA h g^{-1}.

The benefit of adding tin oxide to carbon nanofibers is more evident at charge densities greater than 50 mA g^{-1} (Figure 6d). The 10th cycle discharge capacity of the C-SnO_2 composite is greater than the pure carbon fibers by as much as 150 mA h g^{-1}. At higher charge rates, lithium insertion may be diffusion limited. Thus, the tin oxide-carbon fibers can accommodate more lithium atoms at outer surfaces of the fibers than for pure carbon, which allow for greater accessibility of the lithium during rapid rates of charging. Consequently, the addition of tin salt to the PAN nanofibers leads to an alloy material (i.e., SnO_2) for lithium, as well as a more beaded fiber morphology, both of which may account for the improved properties.

After cycling, mats were removed from the batteries and rinsed with acetone to remove any residual electrolyte. Micrographs shown in Figure 7a and b reveal that the structures of C-SnO_2 and carbon fibers were maintained despite lithium intercalation. Contrary to what has been previously reported with other nanofiber mats, fibers were not damaged and did not show signs of powderization.[18] The ability of the fibrous mats to remain intact during cycling confirms that binders are not needed with the composite and pure carbon nanofibrous anodes.

2.1. Nanofibers Surface-Loaded with SnO_2 Nanoparticles via Soak Treatment. The goal for this part of the study was to enhance the tin oxide content incorporated within the nanofibers during electrospinning with a surface enrichment soaking method. Although the benefits of the first approach included minimal process steps, the content of tin within the fibers was limited by the solubility of tin sulfate in electrospinning solutions and conversion of tin oxide from heat treatments. In our second approach, nanofiber mats were soaked in aqueous tin salt solutions, because tin sulfate has a higher solubility in water than DMF.[43] The PAN-based mats were thermally treated in air prior

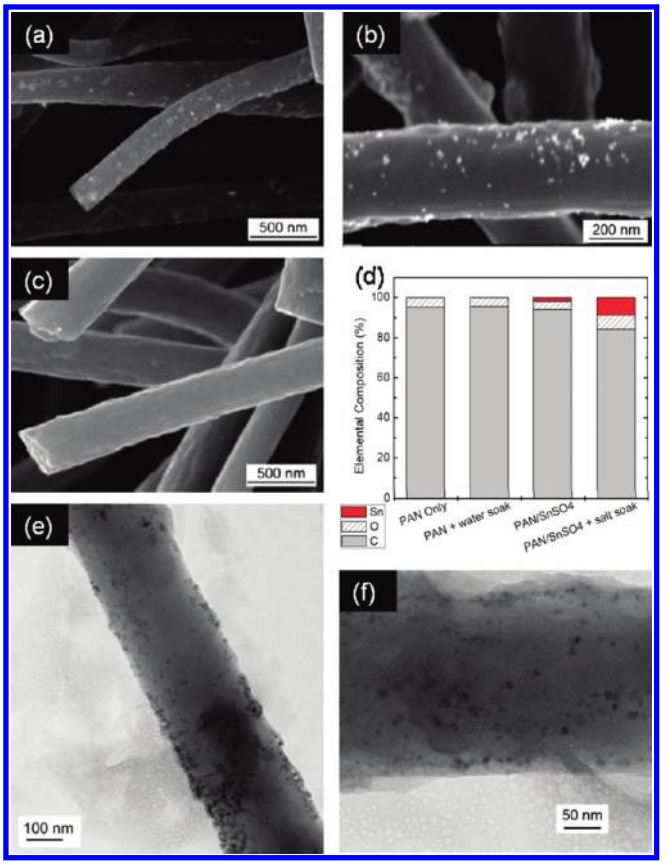

Figure 8. (a, b, e, f) Scanning and transmission electron micrographs of PAN/$SnSO_4$ nanofibers that have been stabilized, soaked in aqueous tin sulfate, and then carbonized to form C-SnO_2 composites. (c) Micrograph of PAN nanofibers that have been stabilized, soaked in water, and then carbonized. The samples were not sputtered-coated. (d) The corresponding elemental composition of the anode mats as measured by EDS.

to the salt infiltration, which oxidized the nanofiber outer surfaces.[34] Compared to PAN, the stabilized polymer is more hydrophilic, which enhances coverage and penetration of disassociated salt particles on the nanofiber exteriors. Furthermore, the stabilized mats are more feasible to handle and soak compared to the more flexible, electrospun PAN mat, which can fold over on itself in solution.

2.2. Characterization of Stabilized, Salt-Soaked, and Carbonized Nanofibers. The benefits of the soaking treatment are evident from SEM and TEM analysis on the carbonized fibers (Figure 8). PAN/$SnSO_4$ nanofibers that had been soaked in the tin salt solution and carbonized were covered with particles. Individual particles (~15 nm diameter) and particle aggregates (up to ~200 nm) were present on fibers throughout the mat, which confirmed the efficacy of the soak treatment. (Figure 8a, b, e, f.) Prior to SEM and TEM analysis, the particle-loaded mats were rinsed with ethanol or soaked in water in order to verify particle attachment onto the fibers. Both TEM and Raman analysis (discussed later) seem to suggest penetration of the particles below the nanofiber surface, consistent with recent work reported.[26] However the extent of penetration is unclear and falls beyond the realm of this work. In comparison to the salt-soaked fibers, particles were not seen on the surfaces of the control, PAN nanofibers soaked in water prior to carbonization. To characterize

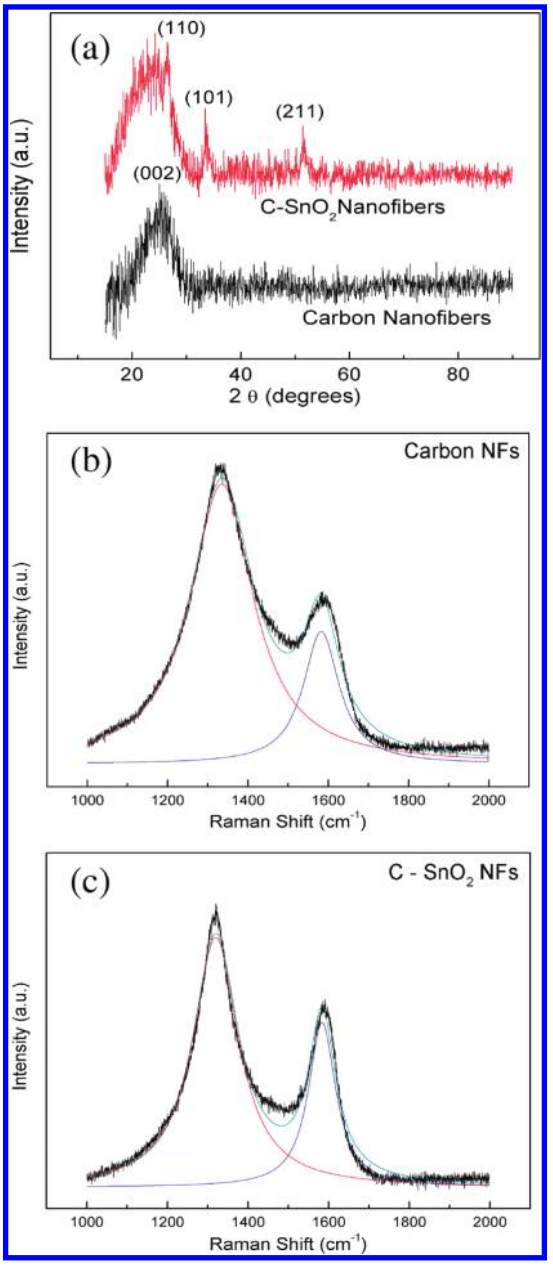

Figure 9. (a) X-ray diffraction patterns of fibers after soak and carbonization heat treatments. Peaks in the composite fiber mats correspond to SnO_2 (JCPDS no. 41−1445). Raman spectra of soaked and carbonized (b) PAN/$SnSO_4$ and (c) PAN nanofiber mats. Height ratios $I(D)/I(G)$ are 1.9 ± 0.1 and 1.5 ± 0.1, respectively. The formation of the tin oxide nanoparticles during the heat treatment may disrupt the carbon microstructure, causing more disorder as indicated by the peak ratio.

the elemental content of each type of mat, the fibers were evaluated quantitatively by SEM-EDS. (Figure 8d) The tin soak treatment increased the tin content in the C-SnO_2 fibers by more than 4 times, up from 1.9 to 8.6 wt %, compared to the composite mats in the first study. No tin was present in the control carbon mats from either study.

In addition to analysis by electron microscopy, the crystal structures of the solution-soaked nanofibers were characterized with XRD. Nanofiber mats were analyzed after soaking in solutions and carbonization. Figure 9a reveals that the XRD pattern of the composite mats had prominent peaks matching tin oxide reflections (JCPDS no. 41−1445), which is consistent with the results of the first approach. In addition, the heat-treated nanofiber mats have peaks at $2\theta = 25°$, corresponding to the (002) reflection of disordered carbon.

Raman analysis revealed structural differences between the solution-soaked carbon and C-SnO_2 nanofibers. As seen in the first approach, the D and G peaks are present in the spectra of the carbonized fibers at ∼1335 and ∼1580 cm^{-1}, respectively (Figure 9b, c). In addition, the pure carbon nanofibers had the same height ratio ($R = 1.5$) as the carbon nanofibers in the first approach, despite the soak treatment and different heating conditions. However, one difference between the carbon nanofibers was the D peak width. The soaked carbon nanofibers had a narrower average width (141 ± 45 cm^{-1}) than the carbon nanofibers without the soak (215 ± 32 cm^{-1}) from the first approach. A broader peak may indicate a greater distribution of aromatic cluster sizes and/or aromatic rings without six carbons.[36] These structural differences may account for differences in anode performance, which will be discussed in the next section.

The tin salt solution soaking treatment significantly affected the carbon microstructure of the composite nanofibers. Most notably, the peak ratio was 1.9, which is the greatest of any of the carbonized samples studied. We hypothesize that the infiltration of the tin salt and subsequent formation of tin oxide particles on and within the nanofibers disrupted the formation of carbon ring clusters. The salt soaking treatment increases the tin content in the composite fiber, which can explain the difference in Raman analyses between the two approaches.

2.3. Performance of Soaked Carbon-SnO_2 Nanofiber Mats as Li-Ion Battery Anodes. The nanofiber mats surface-loaded with tin oxide nanoparticles were evaluated as Li-ion battery anodes. The salt soaking treatment enhances the anode performance, relative to the water-soaked carbon nanofiber control. As observed from Figure 10a and b, the composite fiber mat achieves a first discharge capacity of 788 mA h g^{-1}, which is a 200 mA h g^{-1} improvement over the carbon nanofibers. The added tin content from the salt soak treatment contributed to the enhanced capacity. Both materials have similar first cycle Columbic efficiencies (70%), which can be attributed to the formation of the SEI film on the nanofiber surfaces. For C-SnO_2 fibers, lithium was also lost during the reaction with SnO_2 to form Sn (eq 2). The advantages of the salt soak are also apparent in the cycle life performance (Figure 10c). With a current density of 50 mA g^{-1}, the composite SnO_2-carbon fiber mats maintains a higher capacity than the pure carbon fiber mats for the duration of the test. At the 40th cycle, the capacity of the composite mat is 50 mA h g^{-1} greater than the control mat. On the absis of n our estimates, the theoretical capacity of a composite containing ∼9% Sn is approximately 650 mA h g^{-1}. We note that the soaked C-SnO_2 mats performed above their theoretical capacity for the first cycle (751 mA h g^{-1}), which we attribute to the lithium consumed to form to the SEI film and in the irreversible reaction with SnO_2 (eq 2). The capacities of subsequent cycles (637 mA h g^{-1} (2nd); 495 mA h g^{-1} (10th); 442 mA h g^{-1} (40th)) are below the calculated theoretical capacity. We believe that that this capacity loss is caused by structural breakdown of the nanostructured electrode during lithium de/insertion, as well as lithium that is retained within the electrode by incomplete dealloy reaction.

A comparison of our C-SnO_2 composites with other electrospun nanofiber electrodes reported in the literature reveal

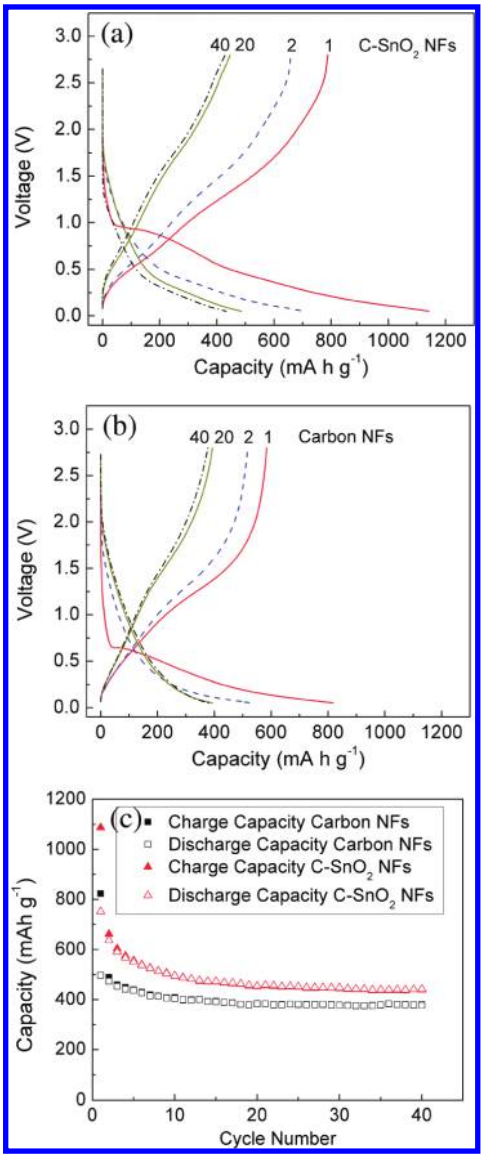

Figure 10. Charge−discharge curves for (a) pure carbon nanofibers, soaked in water prior to carbonization, and (b) SnO2-carbon nanofibers, soaked in salt solution prior to carbonization. (c) Cycle life of carbon−tin oxide and carbon nanofiber mats with solution soak treatments. The anodes were cycled with a constant 50 mA g^{-1} current density.

interesting features. For instance, carbon−silicon anodes in studies conducted by our group[19,23] had higher capacities than C-SnO_2, but less efficient cycle lives. In addition to the lithium alloy, one difference between the two materials is the size and distribution of nanoparticles on/within the nanofibers. Specifically, large (>1 μm) silicon particle aggregates were on the same size order as the carbon fiber diameters. The stresses within the composite electrode caused by volume changes within the aggregated lithium alloys likely contributed to the decay in capacity.[1] In addition, the cycle stability of our C-SnO_2 anodes was similar to other carbon-Sn composite nanofibers,[24−27] with Coloumbic efficiencies more than 90% after the second cycle. Recently, Zou et al. conducted systematic studies on the fabrication carbon nanofibers containing tin and tin oxide nanoparticles, which were also evaluated in lithium ion half cells without a binder or conductive additives.[25,26] The capacities of the carbon−tin anodes in their studies were comparable to our C-SnO_2 materials. We note that differences in the methodology, including materials and process conditions, as well as the battery cycling conditions (i.e., cycling rate, voltage) make a direct comparison not viable. Nevertheless, these studies, together with ours provide further evidence of the promise of carbon−tin electrospun composites as anode materials.

Although the benefits of the added tin oxide to the nanofiber anodes are evident in this study, the capacities are reduced, as compared to the mats in the first study. Most notably, the 10th cycle capacities of pure carbon fiber mat that were soaked in water are more than 100 mA h g^{-1} lower than the pure carbon fiber mats from the first study. We hypothesize that changes to the thermal treatment, from one continuous to two separate cycles (to accommodate the soak treatment), led to the reduction in capacities. This is because the process of separating the heat steps in the second study (25 °C → 280 °C, soak at 25 °C, 25 °C → 600 °C) exposes the mats to a longer combined thermal treatment than the continuous process in the first study (25 °C → 280 °C → 600 °C). We speculate that these differences in the thermal treatments affect the material properties of the mats, by altering the carbon microstructures within the nanofibers. Structural differences between the carbon nanofibers in the two studies are evident in the Raman analysis. Specifically, the carbon nanofibers in the second study had a smaller size distribution of carbon-ring clusters. Thus, the carbon structure within the nanofibers in the second study may have more order compared to the first study, and in turn, a lower storage capacity for lithium.[38] We are pursing further studies to investigate the role of continuous and separated thermal treatments on the carbon structure in PAN-based nanofibers and their performance as anodes.

Although the heat treatment process conditions may require further optimization to maximize anode performance (not the goal of this study), the benefits of the salt soak treatment compared to the control are evident. The infiltration of tin salts into fiber mats by soak treatments is a facile route to loading tin oxide particles onto nanofiber surfaces. We conceive that this technique can be combined with the incorporation of other nanoparticles that form lithium alloys during electrospinning to further enhance the performance of these materials as Li-ion battery anodes.

CONCLUSIONS

We found that tin oxide can be incorporated into carbon nanofibers, which improves their performance when evaluated as lithium ion battery anodes. The addition of tin sulfate to polymer nanofibers (1) during and (2) after electrospinning, followed by heat treatments, were two facile methods to prepare the C-SnO_2 composites. The latter approach yielded a greater concentration of tin, since tin sulfate has a higher solubility in the soaking solution (water) than the electrospinning solution (DMF). X-ray diffraction and energy dispersive spectroscopy confirmed the formation of tin oxide after the heat treatments. In addition, Raman analysis revealed that the addition of the soaking treatment (Approach #2) led to a more disordered carbon structure than the first approach with one continuous heat treatment.

ASSOCIATED CONTENT

Supporting Information. Thermal gravimetric analysis of tin sulfate decomposition during stabilization and

carbonization heat treatments. This material is available free of charge via the Internet at http://pubs.acs.org.

AUTHOR INFORMATION

Corresponding Author
*E-mail: khan@eos.ncsu.edu. Phone: 919-515-4519.

ACKNOWLEDGMENT

This work was supported by National Science Foundation GOALI Program (#0555959) and a Department of Education GAANN Fellowship (CAB). The authors thank Professor Peter S. Fediw and Andrew Loebl for helpful discussions.

REFERENCES

(1) Winter, M.; Besenhard, J. O.; Spahr, M. E.; Novak, P. *Adv. Mater.* **1998**, *10*, 725–763.
(2) Besenhard, J. O.; Yang, J.; Winter, M. *J. Power Sources* **1997**, *1*, 87–90.
(3) Wilson, A. M.; Dahn, J. R. *J. Electrochem. Soc.* **1995**, *2*, 326–332.
(4) Tarascon, J. M.; Armand, M. *Nature* **2001**, *6861*, 359–367.
(5) Kim, C.; Yang, K. S.; Kojima, M.; Yoshida, K.; Kim, Y. J.; Kim, Y. A.; Endo, M. *Adv. Funct. Mater.* **2006**, *18*, 2393–2397.
(6) Ding, Y. H.; Zhang, P.; Long, Z. L.; Jiang, Y.; Xu, F.; Di, W. *Sci. Technol. Adv. Mater.* **2008**, 1–5.
(7) Cho, T. H.; Sakai, T.; Tanase, S.; Kimura, K.; Kondo, Y.; Tarao, T.; Tanaka, M. *Electrochem. Solid-State Lett.* **2007**, *7*, A159–A162.
(8) Bonino, C. A.; Krebs, M. D.; Saquing, C. D.; Jeong, S. I.; Shearer, K. L.; Alsberg, E.; Khan, S. A. *Carbohydr. Polym.* **2011**, 111–119.
(9) Saquing, C. D.; Manasco, J. L.; Khan, S. A. *Small* **2009**, *8*, 944–951.
(10) Talwar, S.; Hinestroza, J.; Pourdeyhimi, B.; Khan, S. A. *Macromolecules* **2008**, *12*, 4275–4283.
(11) Talwar, S.; Krishnan, A. S.; Hinestroza, J. P.; Pourdeyhimi, B.; Khan, S. A. *Macromolecules* **2010**, *18*, 7650–7656.
(12) Tang, C.; Saquing, C. D.; Harding, J. R.; Khan, S. A. *Macromolecules* **2010**, *2*, 630–637.
(13) Huang, Z. M.; Zhang, Y. Z.; Kotaki, M.; Ramakrishna, S. *Compos. Sci. Technol.* **2003**, *15*, 2223–2253.
(14) Li, D.; Xia, Y. N. *Adv. Mater.* **2004**, *14*, 1151–1170.
(15) Arico, A. S.; Bruce, P.; Scrosati, B.; Tarascon, J. M.; Van Schalkwijk, W. *Nat. Mater.* **2005**, *5*, 366–377.
(16) Li, N.; Martin, C. R. *J. Electrochem. Soc.* **2001**, *2*, A164–A170.
(17) Ji, L. W.; Zhang, X. W. *Electrochem. Commun.* **2009**, *4*, 795–798.
(18) Wang, L.; Yu, Y.; Chen, P. C.; Zhang, D. W.; Chen, C. H. *J. Power Sources* **2008**, 717–723.
(19) Ji, L. W.; Zhang, X. W. *Electrochem. Commun.* **2009**, *6*, 1146–1149.
(20) Ji, L. W.; Lin, Z.; Medford, A. J.; Zhang, X. W. *Chem.—Eur. J.* **2009**, *41*, 10718–10722.
(21) Ji, L. W.; Jung, K. H.; Medford, A. J.; Zhang, X. W. *J. Mater. Chem.* **2009**, *28*, 4992–4997.
(22) Ji, L. W.; Lin, Z.; Guo, B. K.; Medford, A. J.; Zhang, X. W. *Chem. —Eur. J.* **2010**, *38*, 11543–11548.
(23) Ji, L. W.; Zhang, X. W. *Carbon* **2009**, *14*, 3219–3226.
(24) Yu, Y.; Gu, L.; Wang, C. L.; Dhanabalan, A.; van Aken, P. A.; Maier, J. *Angew. Chem., Int. Ed.* **2009**, *35*, 6485–6489.
(25) Zou, L.; Gan, L.; Kang, F.; Wang, M.; Shen, W.; Huang, Z. *J. Power Sources* **2010**, 1216–1210.
(26) Zou, L.; Gan, L.; Lv, R. T.; Wang, M. X.; Huang, Z. H.; Kang, F. Y.; Shen, W. C. *Carbon* **2011**, *1*, 89–95.
(27) Yu, Y.; Gu, L.; Zhu, C. B.; van Aken, P. A.; Maier, J. *J. Am. Chem. Soc.* **2009**, *44*, 15984–15985.
(28) Cueilleron, J.; Hartmanshenn, O. *Bull. Chem. Soc. Fr.* **1959**, *1*, 168–172.
(29) Courtney, I. A.; Dahn, J. R. *J. Electrochem. Soc.* **1997**, *6*, 2045–2052.
(30) Lee, K. T.; Lytle, J. C.; Ergang, N. S.; Oh, S. M.; Stein, A. *Adv. Funct. Mater.* **2005**, *4*, 547–556.
(31) Fong, H.; Chun, I.; Reneker, D. H. *Polymer* **1999**, *16*, 4585–4592.
(32) Phadke, M. A.; Musale, D. A.; Kulkarni, S. S.; Karode, S. K. *J. Polym. Sci., Part B: Polym. Phys.* **2005**, *15*, 2061–2073.
(33) Edie, D. D. *Carbon* **1998**, *4*, 345–362.
(34) Rahaman, M. S. A.; Ismail, A. F.; Mustafa, A. *Polym. Degrad. Stab.* **2007**, *8*, 1421–1432.
(35) Mittal, J.; Bahl, O. P.; Mathur, R. B. *Carbon* **1997**, *8*, 1196–1197.
(36) Ferrari, A. C.; Robertson, J. *Phys. Rev. B: Condens. Matter. Mater. Phys.* **2000**, *20*, 14095–14107.
(37) Zussman, E.; Chen, X.; Ding, W.; Calabri, L.; Dikin, D. A.; Quintana, J. P.; Ruoff, R. S. *Carbon* **2005**, *10*, 2175–2185.
(38) Kim, C.; Park, S. H.; Cho, J. K.; Lee, D. Y.; Park, T. J.; Lee, W. J.; Yang, K. S. *J. Raman Spectrosc.* **2004**, *11*, 928–933.
(39) Arora, P.; White, R. E.; Doyle, M. *J. Electrochem. Soc.* **1998**, *10*, 3647–3667.
(40) Eshkenazi, V.; Peled, E.; Burstein, L.; Golodnitsky, D. *Solid State Ionics* **2004**, *1—2*, 83–91.
(41) Aurbach, D. *J. Power Sources* **2000**, *2*, 206–218.
(42) Winter, M.; Besenhard, J. O. *Electrochim. Acta* **1999**, *1—2*, 31–50.
(43) Haynes, W. M., In *CRC Handbook of Chemistry and Physics*, 91st ed.; Taylor & Francis: Boca Raton, FL, 2010.